Interchain Packing in Bisphenol A Polycarbonate

Patricia Lani Lee,† Tomasz Kowalewski, Mark D. Poliks,‡ and Jacob Schaefer*

Department of Chemistry, Washington University, St. Louis, Missouri 63130

Received November 11, 1994; Revised Manuscript Received January 10, 1995®

ABSTRACT: Bisphenol A polycarbonates prepared with varying thermal history have been examined by dynamic mechanical spectroscopy (DMS), differential scanning calorimetry (DSC), and nuclear magnetic resonance (NMR). The results are consistent with a description of interchain packing in polycarbonate based on local regions of aligned chains referred to as bundles. In this model, two distinct types of cooperative, interchain motions are possible: those of chains within one bundle and those of one bundle relative to another. We believe that low-frequency DMS (tan δ at 0.01 Hz) and stress-relaxation DMS (at 10 s) identify a loss peak at −120 °C arising from intrabundle motion and another at −80 °C due to interbundle motion. Results from DMS, DSC, and dipolar rotational spin-echo ^{13}C NMR suggest that acetone-induced crystallization suppresses intrabundle motions, while residual acetone enhances interbundle motions. Interpretation of residual-proton NMR of perdeuterated polycarbonate leads to the conclusion that interbundle motions are sensitive to thermal history and that annealing at $T < T_g$ reduces interbundle spacing.

The predominant molecular motion in polycarbonate is 180° flips of the phenyl rings.[1−3] Although the ring flips themselves are energy conserving, the lattice reorganization[4] that is necessary to accommodate the motion is able to dissipate energy. The cooperative motion between polymer chains required by the ring flips means that *inter*molecular interactions play a dominant role in determining macroscopic properties. To study chain packing in polycarbonate and its effect on mechanical properties, we have examined samples of varying thermal history using three techniques: dynamic mechanical spectroscopy (DMS), differential scanning calorimetry (DSC), and nuclear magnetic resonance (NMR). The DMS and DSC experiments are sensitive to global, bulk molecular motions and phase transitions. The NMR experiment depends on localized structure and dynamics and differentiates between motions at specific chemical sites. Combination of the results from these three techniques allows for a description of the interchain packing in polycarbonate that cannot be inferred from one technique alone.

Experiments

Dynamic Mechanical Spectroscopy. Experiments were carried out in tension mode using a Rheometrix RSA II dynamic mechanical tester equipped with a low-temperature unit using liquid nitrogen as a cooling medium. The instrument was modified slightly to prevent artifacts at subzero temperatures caused by ice buildup on the upper sample fixture. This was done by shielding the upper fixture from air from the bearings and flushing the portion of the fixture exterior to the oven with dry nitrogen. Most of the measurements were performed in the temperature range 135−300 K, thus avoiding annealing effects due to heating the samples above their storage temperature. To minimize the well-known contribution of sorbed atmospheric water to the dynamic mechanical behavior of polycarbonate,[5] samples were stored in small closed vials containing anhydrous $CaSO_4$. The vials were kept at room temperature in a vacuum oven (~1 mTorr). The samples were exposed to air for no more than 30 s during mounting prior to the mechanical tests, which were performed in an atmosphere of nitrogen.

The tan δ measurements were performed in the frequency range of 0.01−16 Hz. The temperature was stepped in 5 °C intervals. Maxima of tan δ curves were determined from fifth-degree polynomial least-squares fits in the range ±30 °C around relaxation maxima. The tan δ measurements at 0.01 Hz were determined as averages of multiple measurements at each temperature for increased sensitivity.

The samples used for tan δ measurements were remounted in sample fixtures at room temperature and cooled at constant length to −140 °C. After equilibration, stress-relaxation measurements were carried out in 5 °C intervals. A load of 500 g was applied instantaneously and the stress-relaxation response sampled at a rate of 10 points/s. Each experiment was repeated three times with a reproducibility of better than 5%. Static stress−strain measurements confirmed that all sample deformations remained within the linear range of stress−strain behavior. After incrementing the temperature, the sample−fixture separation was adjusted with the aid of a strain-offset control to compensate for thermal dilatation. These displacements were used in the determinations of the vertical-shift parameters for construction of the relaxation master curve. Stress-relaxation behavior on a time scale longer than several tens of seconds exhibited irregular oscillations probably caused by temperature-induced variations along the sample length. The first 10 s of relaxation behavior was reproducible.

Differential Scanning Calorimetry. DSC experiments were performed using a DuPont 910 differential scanning calorimeter equipped with a Polymer Laboratories control and data-acquisition system. Melting onsets of indium, tin, and zinc were used for temperature calibration. Analytical samples weighing about 5 mg were crimped in aluminum pans. Measurements were carried out in a static air atmosphere at a scanning rate of 50 °C/min. A high heating rate was used to minimize annealing effects in measurements on nonequilibrium samples. Values of T_g were shifted by about 5 °C relative to those measured at a scanning rate of 10 °C/min. After each experiment the DSC oven was cooled to room temperature using an external liquid-nitrogen bath. Each experiment was performed at least 5 min after placing the sample in an oven to allow for instrument thermal equilibration. Repetitions were separated by at least 1 h.

Nuclear Magnetic Resonance. Protonated aromatic-carbon dipolar line shapes were characterized by dipolar rotational spin-echo 15.1-MHz ^{13}C NMR. This is a two-dimensional experiment in which, during the additional time dimension, carbon magnetization is allowed to evolve under the influence of H−C coupling, while H−H coupling is suppressed by homonuclear multiple-pulse decoupling.[6] Details of the pulse sequence, spectrometer, and dipolar side-band

† Present address: ESPCI, 10, rue Vauquelin, 75231 Paris, France.

‡ Present address: IBM Corporation, Endicott, NY 13760.

® Abstract published in *Advance ACS Abstracts,* March 1, 1995.

0024-9297/95/2228-2476$09.00/0

analysis have been presented before.[2] Solid-state proton NMR was performed using a Chemagnetics CMX300 console with a proton operating frequency of 300 MHz. Magic-angle spinning at 1852 Hz was sufficient to obtain chemical-shift resolution of aromatic, methyl, and residual water signals.[7] Spectra were collected with a $90_x-\tau-180_y-\tau$ pulse sequence, with τ equal to an integral number of rotor periods. The 180° pulse width was 10 μs.

Sample Preparation. Polycarbonate powders were obtained by dropwise precipitation from a chloroform solution (1.5% polymer by weight) into methanol. Melt-pressed samples were prepared from commercial-grade Bisphenol A polycarbonate Lexan 101. Pellets were vacuum dried at room temperature for 24 h, compression molded at 220 °C into a 0.25-mm-thick films between polished, chromium-coated plates, and annealed by cooling freely in the press to room temperature. DSC indicated no crystallinity above 1% for these melt-pressed films. Samples for DMS were cut into strips, 2.5 mm wide by 30 mm long. Semicrystalline samples were obtained by exposing polymer films to saturated vapors of acetone for 1 h. Freshly crystallized films were then dried between chromium-coated plates under a slight load to prevent buckling. These semicrystalline films were subsequently annealed by heating in a vacuum oven at 190 °C for 4 h.

The perdeuterated monomer precursor of polycarbonate-d_{14} was obtained from MSD Isotopes. The average residual proton concentration was 1% by high-resolution solution-state NMR. The ratio of aromatic protons to methyl protons was 2:1 rather than the expected 4:3, indicating that the methyl groups had been preferentially deuterated.[7] Polymerization was performed in two separate reactions, one at Monsanto Co. and the other at Polysciences, Inc. Both samples gave similar results by DSC and proton NMR. The average residual proton concentration remained at 1% after polymerization. The resultant polycarbonate-d_{14} powders were dissolved in chloroform and reprecipitated drop by drop in methanol. The solid was collected by suction filtration, air-dried overnight, and vacuum-dried at 80 °C. The preparation of annealed amorphous, semicrystalline and annealed semicrystalline samples from polycarbonate-d_{14} powder was identical to that described above for fully protonated polycarbonate.

Results

Dynamic Mechanical Spectroscopy. (1) Horizontal-Shift Parameters and Construction of the Master Relaxation Curve. The stress relaxation of polycarbonate is shown in Figure 1 as a set of plots of Young's modulus (E) as a function of the logarithm of time. Measurements in intervals of 5 °C provide enough overlap between the curves to allow a horizontal shift in logarithmic scale such that

$$E^T(\ln \tau) = E^{T_0}(\ln \tau/a_T) \tag{1}$$

where E^{T_0} is the stress relaxation at the reference temperature, T_0, and a_T is the experimentally determined horizontal-shift parameter.[8] For sub-T_g processes,

$$a_T(T) \sim \exp(-E_a/RT) \tag{2}$$

where E_a denotes the activation energy associated with the process.

(2) Vertical-Shift Parameters. As described by McCrum and Morris,[9] construction of the master relaxation curve also involves vertical shifts, compensating for the inherent changes in modulus caused by a change in temperature. This correlation requires the parameters b_T, c_T, and d_T to connect the relaxed modulus (E_R) and the unrelaxed modulus (E_U):

$$E_R{}^T - E_U{}^T = b_T(E_R{}^{T_0} - E_U{}^{T_0}) \tag{3}$$

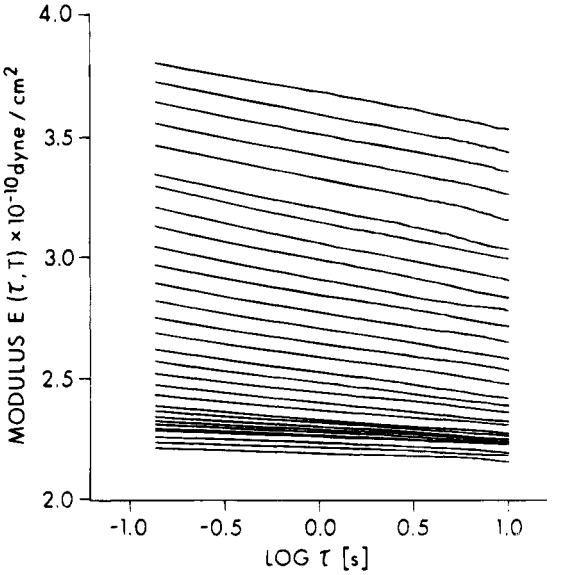

Figure 1. Set of stress relaxation curves for annealed amorphous polycarbonate with temperature increasing (from top to bottom) from −138 to 23 °C in 5 °C intervals. Each relaxation curve represents an average of three consecutive measurements.

$$E_U{}^T = c_T E_U{}^{T_0} \tag{4}$$

$$E_R{}^T = d_T E_R{}^{T_0} \tag{5}$$

where superscripts refer to temperatures T and T_0. We will assume the same temperature scaling for relaxed and unrelaxed moduli so that $b_T = c_T = d_T$.

Vertical-shift parameters can be predicted theoretically only in the case of rubber elasticity.[10] For glassy polycarbonate, we obtained the vertical-shift parameters (c_T) using a procedure that starts with the molar-volume dependence of the bulk modulus, B. This dependence can be derived from a Lennard-Jones potential for the intermolecular force field:

$$B = B_0/6\{15(V_0/V)^5 - 9(V_0/V)^3\} \tag{6}$$

where V is the molar volume and V_0 and B_0 are the molar volume and bulk modulus when the expansion volume is zero. This relationship has been shown to describe the bulk modulus of poly(methyl methacrylate) over a wide range of temperatures and pressures.[11] Next we determined the temperature dependence of B from the experimentally determined coefficient of thermal expansion (obtained from the sample-fixture displacement necessary to correct for dilation). We assumed that Poisson's ratio (ν) was constant throughout the temperature range of interest so that

$$E = 3B(1 - 2\nu) \tag{7}$$

and

$$E(T)/E_0 = B(T)/B_0 \tag{8}$$

The experimentally observed modulus at the end of 10 s for each stress-relaxation experiment is shown in Figure 2 as a function of temperature. This modulus is designated E(10 s). The low-temperature behavior of E(10 s) is associated with the γ relaxation of polycarbonate and the high-temperature behavior with the much slower changes in the modulus due to the tem-

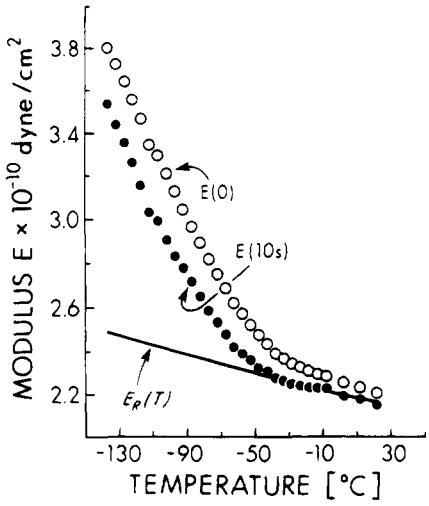

Figure 2. Illustration of the extrapolation of the relaxed modulus to low temperatures, necessary for determination of the vertical-shift parameter, c_T, used in construction of the modulus relaxation master curve. Filled circles correspond to experimental values of the modulus after 10 s, $E(10\ s)$. The solid line shows the temperature dependence of the relaxed modulus, $E_R(T)$, which results from the fit of eqs 6–8 of the text to the high-temperature portion of $E(10\ s)$.

perature variability of the molar volume as described by eq 6. The parameters of eq 6 were therefore fitted to the behavior of the relaxed modulus between −40 °C and room temperature; B_0 and V_0 were determined by a simple fit to $E(10\ s)$ at $T = 20$ °C. The temperature dependence of the molar volume was calculated from the experimentally determined coefficient of linear expansion, assuming a room temperature density $\varrho = 1.2$. Using this dependence and eq 8 leads to the relaxed modulus, $E_R(T)$, shown in Figure 2 as the solid line. Values of the vertical-shift parameter were then calculated using

$$c_T(T) = E_R(20)/E_R(T) \tag{9}$$

where $E_R(20)$ is the value of E_R at 20 °C.

(3) Correction of Stress Relaxation. The vertical-shift parameter was used to correct the experimental stress-relaxation curves, $E(\tau,T)$:

$$E_c(\tau,T) = c_T(T)\,E(\tau,T) \tag{10}$$

Each corrected set of stress-relaxation curves, $E_c(\tau,T)$, was then subjected to the horizontal-shift procedure of eq 1, with −102 °C as the reference temperature, $T_R = T_0$. The curves were shifted by the amount calculated as the average difference between the fifth-degree polynomial fits of overlapping portions of relaxation curves. The resulting master curve for the modulus is shown in Figure 3 (left, solid line) and the Arrhenius plot of shift factors, a_T, in Figure 4 (left).

(4) Numerical Differentiation and the Relaxation Spectrum. The relaxation spectrum (Figure 3, left, dotted line) was determined from the first-approximation relationship:[12]

$$H(\log \tau) = -\mathrm{d}E(\log \tau)/\mathrm{d}(\log \tau) \tag{11}$$

The numerical differentiation of eq 11 is sensitive to noise and requires data smoothing. This was accomplished by three different procedures, all of which produced essentially the same relaxation spectrum. The master curve obtained from the horizontal-shift procedure represents a set of unevenly spaced data, so filtering based on conventional fast Fourier transform techniques could not be applied. Instead, we used an algorithm designed for nonequally spaced data.[13] In a second approach we Fourier-filtered $E_c(\tau,T)$ and $\mathrm{d}E_c(\tau,T)/\mathrm{d}\tau$ separately in the time domain, converted to a logarithmic scale, and then reassembled the relaxation spectrum using the shift factors, a_T. Finally, we performed the numerical differentiation with respect to the logarithm of time by reduction of the original set of data of equally spaced time-domain points into a compressed data set containing only time points spaced in a geometric progression (1, 2, 4, 8, 16, 32, ...).

(5) Secondary Transition. Both stress relaxation (Figure 3, left) and tan δ (Figure 3, right) exhibit a broad secondary transition centered around −100 °C for amorphous annealed polycarbonate. It has been previously established that this transition is due to the lattice rearrangements that accompany ring flips.[4] Translated to room temperature, the transition represents a distribution of frequencies centered around 300 kHz and spanning 5 decades.[2] The transition is actually composed of at least two components (Figure 3, left, dotted line) which in tan δ measurements are resolved only at low frequency (0.01 Hz, Figure 3, right). The multiple-transition character of the γ relaxation peak in polycarbonate has also been observed in experiments involving dielectric relaxation[14] and thermally stimulated currents.[15] In addition, multiple transitions are indicated by the presence of two slopes in the Arrhenius plot of horizontal-shift factors, a_T (Figure 4, left). Based on these slopes the loss peak centered at −120 °C has an activation energy of 45 kJ/mol, while that centered at −80 °C has an activation energy of 65 kJ/mol (Figure 4, left). Near room temperature, the frequencies of the two relaxations converge (Figure 4, right, dotted lines). Extrapolation of higher frequency data for the combined peak to room temperature results in an overestimate of the room-temperature frequency compared to extrapolations of the stress-relaxation data (Figure 4, right, solid line compared to dotted lines).

(6) Acetone-Induced Crystallization. Unlike the situation for the annealed amorphous sample, DMS of the semicrystalline sample changes as the sample ages and the acetone content is reduced (Figure 5a,c). Initially, the DMS spectrum of the semicrystalline sample shows primarily a higher temperature peak in the secondary transition region (Figure 5a). Over time, this peak decreases in amplitude and a lower-temperature peak grows (Figure 5b). After annealing of the semicrystalline sample at 190 °C, the higher temperature peak is reduced to a shoulder (Figure 5c), and the DMS loss peaks appear at the same temperatures as the corresponding peaks in the amorphous polycarbonate. Data for the semicrystalline sample were obtained with an applied frequency of 16 Hz, and so the multiple transitions observed for the annealed amorphous sample at −120 and −80 °C (with an applied frequency of 0.01 Hz) are not resolved.

Differential Scanning Calorimetry. Before annealing, the melting range of semicrystalline polycarbonate is broad (Figure 5d,e), suggesting that crystallites are small and dispersed so that the delineation between amorphous and crystalline regimes is indistinct. The T_g transition is also indistinct and appears near 100 °C (Figure 5d), which points to plasticization by the residual solvent. After annealing, T_m sharpens and T_g is better defined and shifts to higher temperature

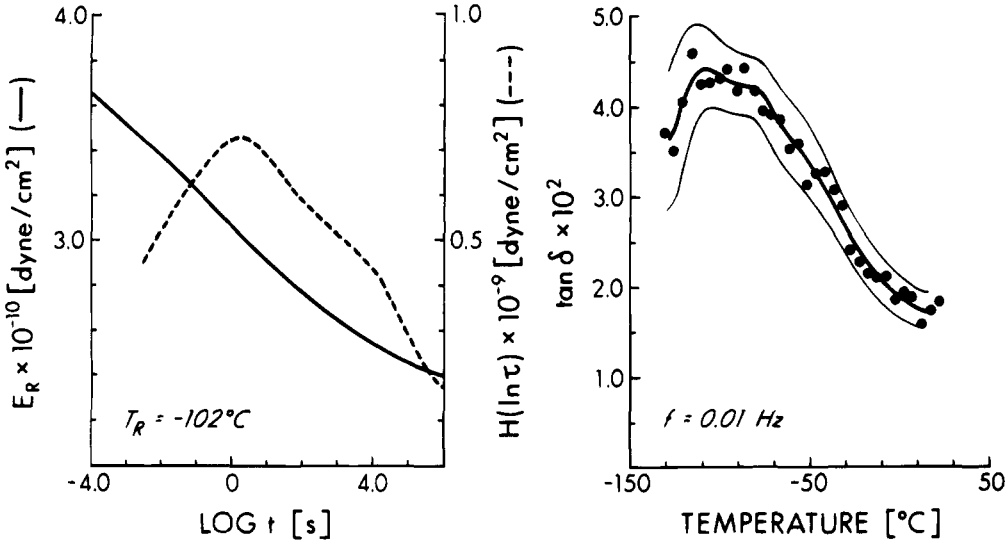

Figure 3. Dynamic mechanical spectra of annealed amorphous polycarbonate. The left panel shows the stress-relaxation master curve for a reduced temperature of −102 °C. In a few instances vertical and horizontal shifts of stress relaxation curves from Figure 1 did not produce perfect overlap due to anomalies in the latest stages of relaxation caused by temperature instability. Appropriately shorter portions of stress-relaxation curves were used in such cases. The dashed line is the first derivative of the solid line. The tan δ at an applied frequency of 0.01 Hz is shown on the right. The individual data points were fit piecewise to a polynomial (heavy center line). Upper and lower error-bar limits are estimates (narrow outer lines).

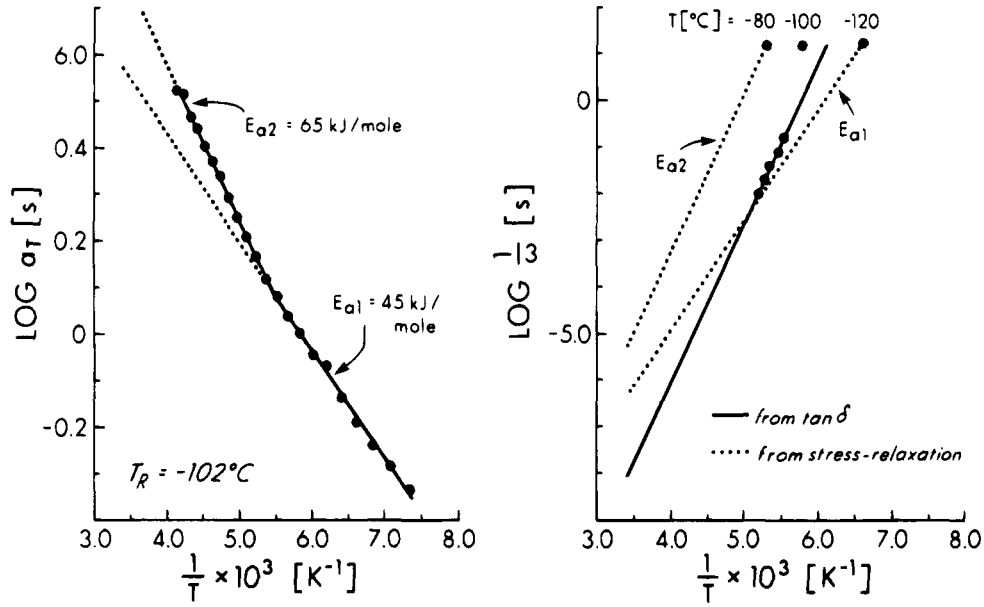

Figure 4. (Left) Activation energies of low-temperature processes in annealed amorphous polycarbonate calculated from the a_T shift factors; E_{a1} corresponds to the loss peak at −120 °C, and E_{a2} corresponds to the loss peak at −80 °C. (Right) Extrapolation of activation energies to room temperature (dotted lines). The solid line represents activation energy as determined by tan δ at 1−16 Hz.

(Figure 5e,f), indicating the existence of better-defined crystalline and noncrystalline domains and removal of the plasticizing solvent residues.

The small exotherm in the middle of the glass transition (solid bold line) observed in the DSC of polycarbonate powder (Figure 6) suggests the relaxation of high-energy conformations[16] that were trapped during the precipitation process. Near T_g there is apparently enough molecular motion for these unfavorable conformations to rearrange to a more thermodynamically stable state which is accompanied by the observed exotherm. These high-energy extended conformations, originally trapped when the polymer went from solution in a good solvent to a precipitated powder, do not reform in the melt, and so no exotherm appears during the second heating (dashed line). The annealed amorphous sample shows no exotherm during T_g (solid line); the post-T_g endotherm is characteristic of annealed materials.[12]

Nuclear Magnetic Resonance. Dipolar rotational spin-echo sideband intensities (15.1 MHz) (normalized to the $n = 1$ first spinning side band) are presented in Table 1 for powder, annealed amorphous and annealed semicrystalline polycarbonates. Side-band intensities for powder and annealed amorphous samples are indistinguishable. The n_2/n_1 ratios, for example, are each 0.51. The corresponding n_2/n_1 ratio for the semicrystalline polycarbonate is 0.61, an increase of about 20%.

Figure 7 shows the 300-MHz residual proton NMR spectrum of a polycarbonate-d_{14} powder. Aromatic and residual water signals are resolved, and that of the methyl protons is partially resolved. The position of the

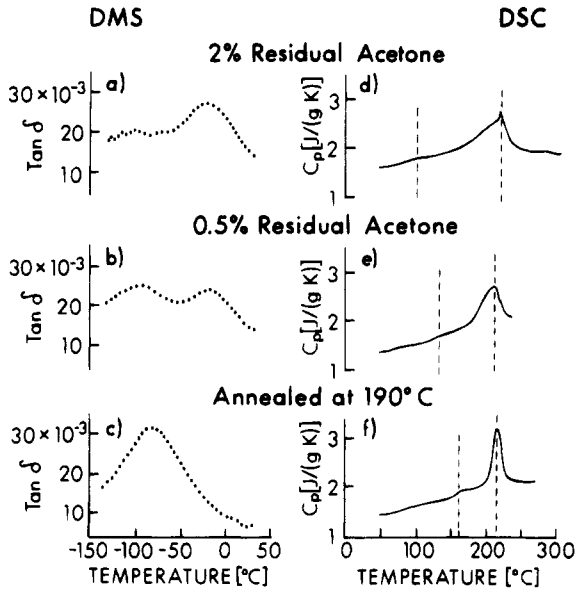

Figure 5. Dynamic mechanical spectra (a–c) and differential scanning calorimetry (d–f) of semicrystalline polycarbonate as a function of residual acetone. The applied frequency for the DMS was 16 Hz. The vertical dashed lines in d–f indicate T_g and T_m.

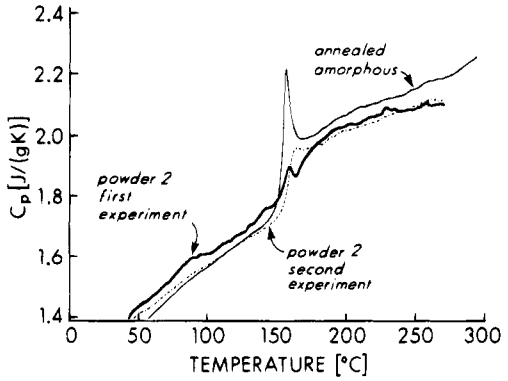

Figure 6. Differential scanning calorimetry of a polycarbonate-d_{14} powder (first experiment, bold solid line; second experiment, dashed line) and annealed amorphous polycarbonate (solid line).

Table 1. Protonated-Aromatic Carbon Dipolar Rotational Spin-Echo 15.1-MHz ^{13}C NMR Side-Band Intensities for Three Polycarbonates under 1859-Hz Magic-Angle Spinning

n	powder	annealed amorphous	semicrystalline (annealed)
0	1.088	1.138	1.113
1	1.000	1.000	1.000
2	0.513	0.505	0.607
3	0.172	0.177	0.219
4	0.049	0.059	0.079
5	0.015	0.016	0.027
6	0.000	0.005	0.001

water resonance is at higher field than that of the methyl protons, consistent with individual water molecules isolated in an organic matrix.[17,18] The results of deuterium-decoupling experiments[7] have shown that the aromatic and methyl-proton spinning side bands of Figure 7 are due to interchain H–D dipolar coupling, while the water side bands arise from intramolecular H–H dipolar interaction. These conclusions are supported by direct measures of the nearest-neighbor, ring-carbon to ring-deuterium distance and the ring-carbon to methyl-deuterium distance by $^2H-^{13}C$ rotational–echo, double-resonance NMR.[19] The frequency-domain

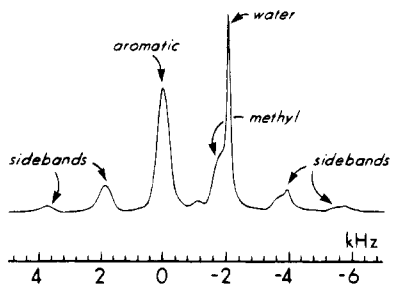

Figure 7. 300-MHz residual proton NMR spectrum of polycarbonate-d_{14} obtained using a $90_x-\tau-180_y-\tau$ pulse sequence, with τ equal to one rotor period. The chemical shift scale is referenced to the aromatic-proton peak at 0 kHz. The small signal that appears at −1 kHz is due to a low-molecular-weight impurity. Magic-angle spinning was at 1852 Hz.

spectra for the annealed amorphous and semicrystalline samples show no significant differences from that of the powder.

Normalized, rotor-synchronized, 300-MHz residual proton, Hahn-echo intensities are shown in Figure 8 for all four polycarbonate-d_{14} samples. The aromatic and methyl-proton T_2's are virtually identical (left and center panels, respectively). The water relaxation varies with sample preparation and is faster in the powder than in the pressed samples (Figure 8, right). Annealing slows relaxation and increases the water T_2 for both semicrystalline and amorphous materials.

Discussion

DMS, Carbon NMR, and the Bundle Model. It has long been acknowledged that all condensed phases, including amorphous glassy polymers, contain short-range molecular order.[20] All of our results are consistent with a description of polycarbonate that allows for small regions of chain alignment[4] which will hereafter be referred to as "bundles". A model of this type for glassy polymers has been proposed by Volkenstein.[21] The concept of bundles has also been used in theoretical studies of cooperative motion in polycarbonate.[22] These bundles, envisioned to consist of perhaps one or two repeat units and approximately nine chains,[23] are defined by the volume within which cooperative motion occurs during the phenyl ring flips. The alignment of these regions is statistical in nature with no crystalline properties. Thus, the order of the glass is short-range (less than 20 Å) and does not perturb the mean end-to-end distance of individual chains. In this model, two distinct types of cooperative, interchain motions are possible: those of chains within one bundle and those of one bundle relative to another.

The dynamic mechanical spectra indeed show two separate low-frequency transitions (Figure 3, left, and Figure 5a,b). Because intrabundle interactions involve smaller motional units which correspond to higher frequencies at lower temperatures, we attribute the lower temperature loss peak to intrabundle reorganization and the higher temperature loss peak to interbundle reorganization. The intrabundle motion is transverse to the chain axis, that is, across the bundle as opposed to down the chain.[22] No conformational changes of the chain need be involved.

The dynamic mechanical spectrum of semicrystalline polycarbonate changes over time as the acetone used to induce the crystallization evaporates. With 2–3% residual acetone present, the low-temperature DMS peak is suppressed by one-third to half (Figure 5a),

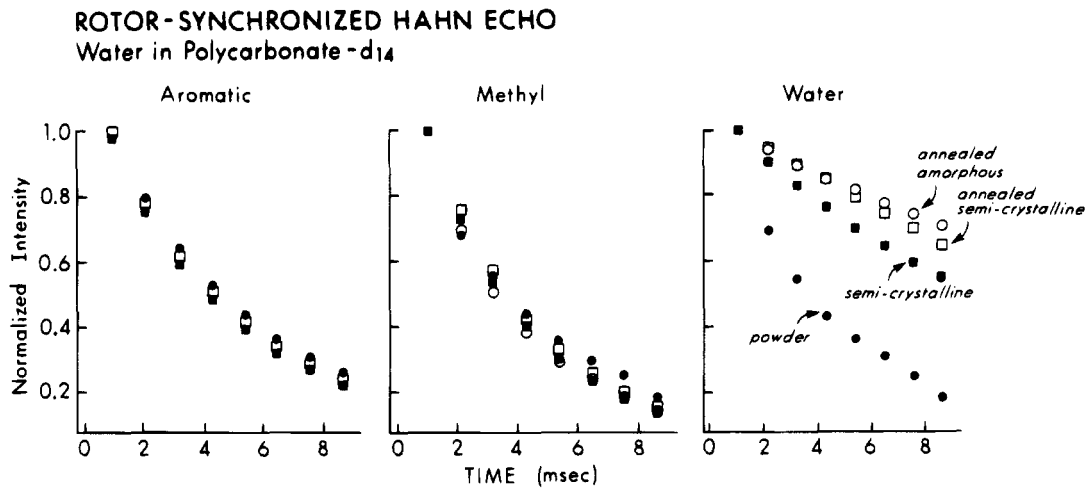

Figure 8. Normalized residual aromatic-proton (left), methyl-proton (center), and absorbed water proton (right) 300-MHz NMR Hahn-echo intensities for polycarbonate-d_{14} obtained using a $90_x-\tau-180_y-\tau$ pulse sequence, with τ equal to an integral number of rotor periods. Magic angle spinning was at 1852 Hz.

indicating a reduction of *intra*bundle motions. Even with only 0.5% acetone present, the low-temperature DMS peak is still reduced by about 20% compared to that of an amorphous sample, consistent with the observed increase in dipolar n_2/n_1 ratio.

The $^{13}C-^{1}H$ dipolar side band n_2/n_1 ratios are 0.50 ± 0.02 for powder and annealed amorphous polycarbonates but 0.61 ± 0.02 for semicrystalline polycarbonate with a low level of residual acetone (Table 1). For a nonflipping ring, we expect an n_2/n_1 ratio of about 1.4; for a flipping ring, we expect a value of 0.5.[24] Thus, all the rings are flipping for the noncrystalline samples. The observed n_2/n_1 ratio of 0.6 for the semicrystalline polycarbonate suggests that on the order of 20% of the rings are not flipping, consistent with the reduction of the low-temperature DMS peak. The nonflipping rings may be blocked by increased rigidity of local chain packing in or near the polycarbonate crystallites or possibly by very low concentrations of trapped residual acetone acting as an antiplasticizer. Because there is more space between the bundles than between chains within bundles, acetone acts as a solvent and plasticizes rather than antiplasticizes the cooperative *inter*bundle motions associated with the high-temperature DMS γ transition, shifting it to −30 °C at 16 Hz (Figure 5a). By this interpretation, as the acetone evaporates, the interbundle motions decrease, the intrabundle motions resume, and the low-temperature loss peak becomes more prominent (Figure 5b,c).

Proton NMR and Bundle Dynamics. The Hahn-echo decay can only arise from modulation of $^{1}H-^{1}H$ or $^{1}H-^{2}H$ dipolar couplings by molecular motion having a correlation time on the order of the rotor period. All other interactions in the perdeuterated polycarbonate are heterogeneous and therefore refocusable by magic-angle spinning. The Hahn−echo NMR experiment measures a reorientation that is thermally activated and so random. Nevertheless, because the reorientation is a slow motion at room temperature, it must involve a large mass in one form or another and therefore must be concerted (or correlated or cooperative—these words are used qualitatively and interchangeably). We identify the large molecular unit with a bundle and the slow motion with reorientation of the bundle axis. These assertions are made within the context of our structural and kinetic model without proof. Our motivation for such assertions is the attempt to rationalize the many connections between NMR relaxation, DMS relaxation, and macroscopic properties which suggest that thermally-activated, small-scale motions in the glass are *indicators* of the local chain packing that is necessary for rapid, stress-induced, large-scale cooperative motion including the initiation of plastic flow.

The polycarbonate T_2's do not depend on thermal history (Figure 8, left and middle panels). In contrast, the water T_2 has a strong dependence on sample preparation (Figure 8, right panel). The low-kilohertz-regime interbundle motions do not change with thermal history, as evidenced by the invariance of the polymer proton T_2's; thus, the differences in water-proton dephasing must arise from changes in the strength of the dipolar coupling.

Changes in water mobility can account for the sample dependence of the water-proton T_2 dephasing. In the powder, water is presumably localized in the densely packed intrabundle regions.[25] In comparison to an annealed sample, we believe that the powder has greater distances between bundles which hinders interbundle jumping of the water molecules. This is also the situation in the amorphous regions of the semicrystalline polycarbonate because residual acetone prevents chains from reaching the equilibrium packing of melt-pressed polycarbonate. Annealing of both semicrystalline and amorphous materials results in more tightly packed configurations which allows the water molecules to jump between bundles more frequently. The increase of water interbundle translational mobility introduces an additional averaging of the dipolar interaction. As a result of weaker dipolar coupling, water T_2 dephasing is reduced in the annealed samples (Figure 8, right panel, open symbols).

Acknowledgment. This work has been supported by NSF Grant DMR-9015864 and by predoctoral fellowships to P.L.L. from the National Science Foundation and the Olin Foundation. We thank Dr. R. J. Kern, formerly of Monsanto Co. (St. Louis), for polymerization of the Bisphenol A-d_{16}.

References and Notes

(1) Spiess, H. W. *Colloid Polym. Sci.* **1983**, *261*, 193.
(2) Schaefer, J.; Stejskal, E. O.; McKay, R. A.; Dixon, W. T. *Macromolecules* **1984**, *17*, 1479.

(3) O'Gara, J. F.; Jones, A. A.; Hung, C.-C.; Inglefield, P. T. *Macromolecules* **1985**, *18*, 1117.
(4) Schaefer, J.; Stejskal, E. O.; Perchak, D.; Skolnick, J.; Yaris, R. *Macromolecules* **1985**, *18*, 368.
(5) Allen, G.; McAinsh, J.; Jeffs, G. M. *Polymer* **1971**, *12*, 85.
(6) Munowitz, M. G.; Griffin, R. G. *J. Chem. Phys.* **1982**, *76*, 2848.
(7) Lee, P. L.; Schaefer, J. *Macromolecules* **1992**, *25*, 5559.
(8) Ward, I. M. *Mechanical Properties of Solid Polymers*; Wiley: London, 1971.
(9) McCrum, N. G. *Anelastic and Dielectric Effects in Polymeric Solids*; Wiley: London, 1967.
(10) Ferry, J. D. *Viscoelastic Properties of Polymers*; Wiley: New York, 1980.
(11) Howard, R. N.; McCallum, J. R. *Polymer* **1971**, *12*, 189.
(12) Rehage, G.; Borchard, W. The Thermodynamics of the Glassy State. In *The Physics of Glassy Polymers*; Haward, R. N., Ed.; Wiley: New York, 1971.
(13) Gorry, P. A. *Anal. Chem.* **1991**, *63*, 534.
(14) Aoki, Y.; Brittain, J. O. *J. Polym. Sci., Polym. Phys. Ed.* **1976**, *14*, 1297.
(15) Aoki, Y.; Brittain, J. O. *J. Polym. Sci., Polym. Phys. Ed.* **1977**, *15*, 199.
(16) Gaur, U.; Wunderlich, B. *Macromolecules* **1980**, *13*, 1618.
(17) Fyfe, C.; Randall, L.; Burlinson, N. *Chem. Mater.* **1992**, *4*, 267.
(18) Derome, A. E. *Modern NMR Techniques of Chemistry Research*; Pergamon Press: Oxford, U.K., 1987; p 34.
(19) Lee, P. L.; Schaefer, J. *Macromolecules*, in press.
(20) Flory, P. J. *Faraday Discuss. Chem. Soc.* **1979**, *68*, 14.
(21) Volkenstein, M. V. *Configurational Statistics of Polymeric Chains*; John Wiley & Sons: New York, 1963; p 544.
(22) Perchak, D.; Skolnick, J.; Yaris, R. *Macromolecules* **1987**, *20*, 121.
(23) Romiszowski, P.; Yaris, R. *J. Chem. Phys.* **1991**, *95*, 6738.
(24) Poliks, M. D.; Schaefer, J. *Macromolecules* **1990**, *23*, 3426.
(25) Lee, P. L.; Xiao, C.; Wu, J.; Yee, A. F.; Schaefer, J. *Macromolecules*, in press.

MA945092P